## Force-Induced Formation of Twisted Chiral Ribbons

Andrew Balchunas, Leroy L. Jia, \*\* Mark J. Zakhary, Joanna Robaszewski, 1,3 Thomas Gibaud, 2vonimir Dogic, 3,1 Robert A. Pelcovits,<sup>5</sup> and Thomas R. Powers<sup>6,5</sup>

<sup>1</sup>The Martin Fisher School of Physics, Brandeis University, 415 South Street, Waltham, Massachusetts 02454, USA <sup>2</sup>Division of Applied Mathematics, Brown University, Providence, Rhode Island 02912, USA <sup>3</sup>Department of Physics, University of California at Santa Barbara, Santa Barbara, California 93106, USA <sup>4</sup>Univ Lyon, ENS de Lyon, Univ Claude Bernard Lyon 1, CNRS, Laboratoire de Physique, F-69342 Lyon, France <sup>5</sup>Department of Physics, Brown University, 182 Hope Street, Providence, Rhode Island 02912, USA <sup>6</sup>School of Engineering, Brown University, 182 Hope Street, Providence, Rhode Island 02912, USA

(Received 21 April 2019; revised 6 March 2020; accepted 12 May 2020; published 30 June 2020)

We demonstrate that an achiral stretching force transforms disk-shaped colloidal membranes composed of chiral rods into twisted ribbons with handedness opposite the preferred twist of the rods. Using an experimental technique that enforces torque-free boundary conditions we simultaneously measure the force-extension curve and the ribbon shape. An effective theory that accounts for the membrane bending energy and uses geometric properties of the edge to model the internal liquid crystalline degrees of freedom explains both the measured force-extension curve and the force-induced twisted shape.

DOI: 10.1103/PhysRevLett.125.018002

Helical shapes are ubiquitous in nature, arising in systems ranging from microscopic assemblages such as collagen, bacterial flagella and lipid bilayer membranes to macroscopic seed pods and the helical structures of the climbing plants [1–9]. Chiral superstructures are also found in diverse synthetic materials including nanoparticle based photovoltaic assemblages and textiles [10-12]. How the microscopic constituents' chirality determines the emergent chiral shape is an important question that underlies all of these phenomena. Besides structural considerations, it is also important to understand how twisted helical shapes deform in response to applied external properties. Generally, an extensile force unwinds a helix, thus reducing its chirality [13–15]. Here, we show that a 2D colloidal membrane twists into a helix under an external force, with twist increasing with extension. The membranes are onerod-length-thick liquid-like monolayers of aligned rods that in the presence of non-adsorbing polymer assemble into diverse structures [16-21]. Depending on the polymer concentration and rod chirality, colloidal membranes form either disks or twisted ribbons [18]. The application of force shifts the relative stability of twisted ribbons and flat colloidal disks. The ribbon phase requires coupling of liquid crystalline order of the constituent chiral rods with the shape of the membrane's edge [22-24]. A quantitative understanding of twisted colloidal ribbons and their mechanical properties might be relevant for understanding the generic pathways by which microscopic chirality is expressed on macroscopic scales.

We first assemble chiral rod-like viruses into equilibrium flat membranes that assume edge energy-minimizing disklike shapes. The rods are perpendicular to the plane of the disk everywhere except near the edge, where they twist with a handedness which is determined by the virus chirality [25]. Surprisingly, we find that pulling on these achiral circular shapes causes them to twist into ribbons. The applied force is achiral, yet it causes the microscopic chirality of the rods to express itself in the macroscopic shape. This observation provides a unique opportunity to study the emergence of force-induced chiral structures for several reasons. First, colloidal membranes have a vanishing zero-frequency inplane shear modulus. Consequently, in contrast to solid elastic sheets, colloidal membranes easily reconfigure, switch between different topologies, and change Gaussian curvature when subjected to external forces. Second, previous work has demonstrated that shapes of colloidal membranes can be modeled with an effective elastic theory in which the bending deformations are described by the Helfrich-Canham free energy [26,27], while liquid-crystalline degrees of freedom of edge-bound rods are described by geometric quantities such as the length, curvature, and geodesic torsion [18,24,25]. Most of the properties that govern these deformation modes have been measured independently thus allowing for rigorous parameter-free tests of theoretical models. For example, colloidal membranes have an intrinsic preference for surfaces with negative Gaussian curvature [21,24]. The Gaussian modulus,  $\bar{\kappa}$ , that controls this preference is important in colloidal and lipid membranes alike, but due to their larger size, slower timescale for shape changes and tendency to form structures with open edges, it is easier to measure  $\bar{\kappa}$  for colloidal membranes. These features enable us to develop a quantitative model that predicts the experimentally observed shape and twist of the colloidal ribbons as a function of applied force, without any adjustable parameters.

We studied membranes assembled from either 0.88  $\mu$ m long fd-wt or 1.2 µm long M13-KO7 viruses that also differ in surface charge [28,29]. At virus concentrations high enough to make a bulk liquid crystalline phase, both viruses form cholesteric phases with a left-handed twist [30]. Adding a depletant changes the phase diagram. Depending on the depletant concentration and the strength of the temperature-dependent chiral interactions, the viruses assemble into either flat disks or twisted ribbons [18]. Confocal microscopy reveals that the force-free ribbons made from fd-wt are right-handed helicoids (see Movie 3 and Fig. S1 of the Supplemental Material [31]). Our experimental setup allowed us to simultaneously apply a known force on a membrane disk and observe its shape [Fig. 1(a)] [31,38]. Two optical traps were produced using an acousto-optical deflector. One trap held the membrane fixed while the other trap placed on the opposite side extended the membrane with well-defined steps. Directly attaching trapped beads to the edge of the colloidal membrane exerted a torque thus precluding accurate measurements of the force-extension curve [Fig. 1(b)]. To generate torque-free boundary conditions we assembled "flagella dumbbells" by binding two streptavidin coated silica beads (2  $\mu$ m diameter) to both ends of a rigid biotin labeled straight flagellar filament isolated from strain SJW

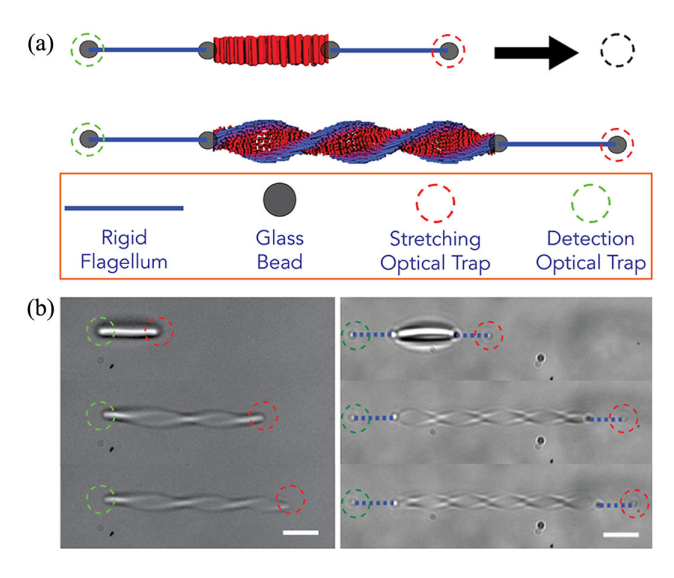


FIG. 1. Stretching a colloidal membrane induces twist. (a) Schematic of a setup that applies a stretching force with a torque-free boundary condition. Side view of flagellar dumbbells attached to an unstretched membrane (top) and a twisted ribbon (bottom). (b) Left: directly trapping colloidal membranes generates an external torque. With increasing extension the ribbon twists when the internal torque generated by the twist overcomes the external torque induced by the optical trap (see Movie 1 of the Supplemental Material [31]). Right: a membrane stretched with flagellar dumbbells twists continuously since the trap is removed from the membrane and symmetric trapped beads freely rotate (see Movie 2 of the Supplemental Material [31]). Dashed circles indicate positions of optical traps. Scale bars, 5  $\mu$ m.

1660 [Fig. 1(b)] [39]. The beads were also coated with an antibody for filamentous viruses which induced strong binding to the membrane edge. Experiments were performed in a microfluidic T chamber where a membraneforming suspension of viruses (100 or 125 mM NaCl and 20 mM tris, pH = 8.15) and Dextran (M.W 500 000) was flowed into the vertical stem. A suspension of biotinylated flagellar filaments, Dextran, streptavidin, and antibody coated silica beads in the same buffer were flowed into the perpendicular arm of the channel. The sample was prepared 24 hours before experiments and kept hydrated to allow colloidal membranes to assemble. Two flagella dumbbell handles were first constructed in the vertical arm using steerable optical traps. Subsequently, using the same traps the "flagella dumbbell" handles were moved to the center of the T stem. One bead of each dumbbell was attached to the opposite sides of an isolated membrane, and the free beads were optically trapped. The dumbbells accurately propagate the applied force due to the large rigidity of flagellar filaments (persistence length ~1 mm) [39].

Using this setup we characterized the response of colloidal membranes to applied force. For any given membrane the measurements were highly repeatable, and there was no hysteresis; we measured the same curve with increasing or decreasing extension [Fig. 2(a)]. However, for different membranes of comparable diameter, measurements had 20% variability in the force extension curve [Fig. 2(a), inset], presumably due to variations in dumbbell attachment to the membranes. The measured force-extension curves exhibited three regimes, with the structures

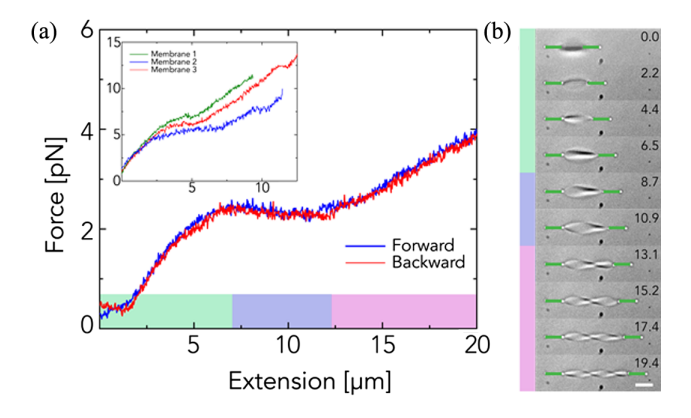


FIG. 2. (a) Measurement of the force-extension curve for a single fd-wt membrane (6.4 mm diameter, 45 mg/ml Dextran and 125 mM NaCl). At low extensions (green bar) the force is directly proportional to extension. At intermediate forces one observes a force plateau (blue bar), and then again a linear increase in force (magenta bar). Inset: Force-extension curves for three different membranes of comparable size ( $\sim$ 6.2  $\mu$ m, 50 mg/ml Dextran, 100 mM NaCl) showing sample to sample measurement variation. (b) Shapes of twisted membrane corresponding to the measured force-extension curve. Extension is given in microns. Scale bar, 5  $\mu$ m.

relaxing to the initial circular membrane when the laser tweezers are shut off. For small extensions, the force increased linearly with extension, and the membrane elongated but exhibited no measurable twist [Fig. 2(b)]. The onset of measurable twist roughly coincided with the appearance of a force plateau, where force hardly changed even as the extension changed by up to several hundred percent. At even higher extension the plateau regime transitioned to a second linear regime [Fig. 2(a)]. The membrane twisted gradually rather than abruptly with extension, and the handedness of the twist was always the same.

We measured how the force-extension curve depends on the diameter for membranes assembled from M13-KO7 virus that have an edge tension of  $\sim 1000~k_BT/\mu m$  [Fig. 3(a)]. The initial slope in the weak force extension

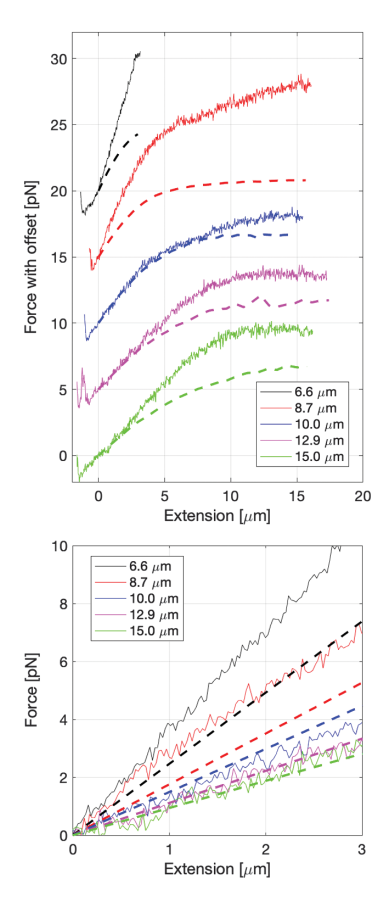


FIG. 3. Membrane diameter determines its stiffness. (a) Experimental force-extension curves (full lines) for colloidal membranes of diameter that increases from 6.6  $\mu$ m to 15.0  $\mu$ m. The membranes are composed of 96% M13-KO7 and 4% M13 wt. For clarity, each membrane is offset by 5 pN. Theoretical predictions (dashed lines) assume the following parameters: edge tension  $\gamma = 1000~k_BT/\mu$ m [18], Gaussian curvature modulus  $\bar{k} = 200~k_BT$  [21], edge moduli  $B = B' = 100~k_BT\mu$ m [18,24] and chiral coupling  $c^* = 50~k_BT$  [24]. (b) First linear regime of the force-extension curves shown in panel (a). Dashed lines are predictions of Eq. (2). Membranes were assembled at 47 mg mL<sup>-1</sup> Dextran, 100 mM NaCl.

regime increased with decreasing membrane size [Fig. 3(b)]. Furthermore, the transition from the plateau to the second linear regime occurred at lower extensions for smaller diameter membranes. Notably, for the smallest membranes, we observed no discernible force plateau as the first and second linear regimes effectively merged. We also examined how the force-extension curve depends on the membrane edge energy. To accomplish this we studied colloidal membranes assembled from fd-wt which had a line tension of  $\sim 380 k_B T/\mu m$  (Fig. 4). The magnitude of the force plateau was dependent on the edge tension, being 2-3 pN for the low tension fd-wt membranes (Fig. 4), and 6-10 pN for the high tension M13-KO7 membranes [Fig. 3(a)]. Finally, our setup allowed us to quantify the spontaneous twist as a function of the extension (Fig. 4, inset) (see Movies 2 and 4 of the Supplemental Material [31]). Since the pitch is defined to be twice the distance between two nodes of the twisted ribbon, it was difficult to measure the pitch at small extensions when there is one or no node.

To understand how extension induces twist, and how the rod twist near the edge relates to ribbon twist, we use an effective model of colloidal membranes which assumes that membrane thickness is small compared to its radius of curvature, and that the membrane size is large compared to the width of the region near the edge where the twist penetrates into the membrane [24]. In this limit the bending energy is given by the Canham-Helfrich energy,  $E_{\rm CH} = (\kappa/2) \int dA(2H)^2 + \bar{\kappa} \int dAK$ , where H is the mean curvature and K is the Gaussian curvature [26,27]. In contrast to

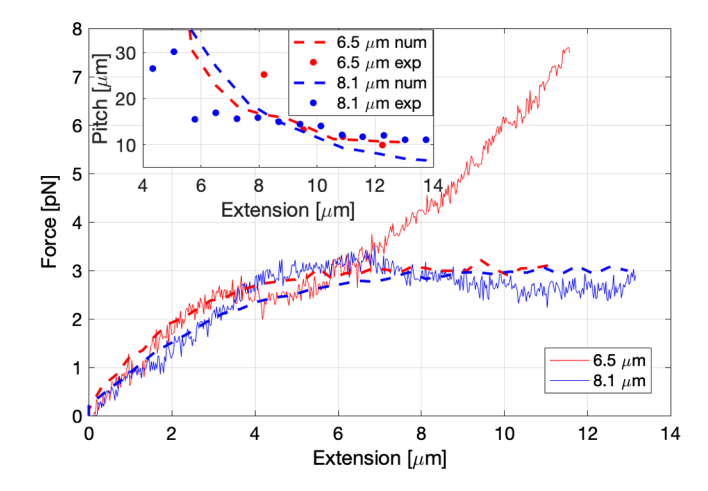


FIG. 4. Experimental data (full lines) and numerical solutions (dashed lines) for force-extension curves for fd-wt membranes with 6.5  $\mu$ m (red) and 8.1  $\mu$ m (blue) diameters (see Movies 2 and 3 in the Supplemental Material [31]). The line tension is 380  $k_BT$   $\mu$ m. Other parameters used in the numerical calculation are the same as those for the M13-K07 membranes. Dextran concentration is 50 mg/mL and 100 mM NaCl. Inset: comparison between experimentally measured (circles) and numerically computed (dashed lines) pitch of the twisted ribbon as a function of membrane extension.

surfactants or lipid bilayers for which  $\kappa$  and  $\bar{\kappa}$  are typically comparable [40,41], experiments and simple models suggest  $\kappa \approx 15,000~k_BT$  [42] while  $\bar{\kappa} \approx 200~k_BT$  [21,24]. Thus, we assume the colloidal membranes in our study only form minimal surfaces (H=0) like planes or helicoids.

We do not explicitly use the Frank free energy on a curved surface [22] to account for rod twist. Instead, since the only contribution to this free energy comes from the thin region near the edge, we use an effective edge energy  $E_{\text{edge}} = \int ds [\gamma + (B/2)k^2 + (B'/2)(\tau_q - \tau_q^*)^2], \text{ where } s \text{ is}$ arclength,  $\gamma$  is the edge tension, k is the edge curvature, Band B' are moduli,  $\tau_q$  is the geodesic torsion (the rate that the surface normal rotates about the edge [43]), and  $\tau_g^*$  is the spontaneous geodesic torsion [24]. For both membrane types,  $B \approx 100 k_B T \mu m$  [18]. This bending rigidity stems from the configuration of the rods near the edge, which twist away from the membrane normal over the characteristic twist penetration length scale, inducing a local in-plane orientational order that resists bending [see [25], and especially Fig. 1(b) of [18]]. We define a chiral coupling  $c^* \equiv -B'\tau_q^*$ , and assume B' = B. To determine the sign of  $\tau_q^*$ , consider a helicoid-shaped membrane [the lower shape of Fig. 1(a)] with pitch p, and let **d** be the rod director field. We suppose that the rods only twist about the axis across the span of the helicoid, with  $\theta$  the angle between the surface normal and d. The twist is

$$\mathbf{d} \cdot \nabla \times \mathbf{d} = \partial_r \theta + \frac{\alpha \sin \theta (\sin \theta + \alpha r \cos \theta)}{1 + \alpha^2 r^2}$$
$$\approx \partial_r \theta + \tau_q \sin \theta^2 + k \sin \theta \cos \theta, \tag{1}$$

where r is the coordinate running along the spanwise direction of the helicoid,  $\alpha = 2\pi/p$ , and the approximation follows because  $\theta$  is small except near the helicoid edge. Now, suppose the rods are chiral with a preference for  $\mathbf{d} \cdot \nabla \times \mathbf{d} > 0$ ; then  $\partial_r \theta$  and  $\tau_g$  are both positive, which means the cholesteric twist of the rods at the edge is left handed, and the twist of the ribbon is right handed, as observed in our experiments on force-free ribbons.

The above described model limits our analysis to the initial linear and plateau regions of the force-extension curve. To solve the model, we assume a surface  $\mathbf{Y}(r,z)=(r\cos\alpha z,r\sin\alpha z,z)$ , where  $0\leq r\leq R(z)$  and  $0\leq z\leq Z$ . Here, Z=2a+z is the stretched length, a is the initial disk radius, and z is the extension; note that vanishing mean curvature implies uniform  $\alpha$ . By the Gauss-Bonnet theorem,  $\int dAK=-\int dsk_g$  (up to a constant), where  $k_g$  is geodesic curvature [44]. Therefore, the problem of finding the optimal membrane surface is reduced to finding the contour on a helicoid that minimizes the energy  $E=E_{\text{edge}}-\int ds\bar{\kappa}k_g$ . We employed a constrained interior-point optimization [45] to solve for the twist rate  $\alpha$  and continuously differentiable curve  $\mathbf{X}(z)=[R(z)\cos\alpha z,R(z)\sin\alpha z,z]$  that minimize E

subject to the constraints of surface area  $\pi a^2$  and length Z. To simplify the analysis, we introduce  $\psi$ , the angle between  $\partial_s \mathbf{X}$  and the r axis [46]:  $(\partial_s R, \partial_s z) = (\cos \psi, -\sin \psi/\sqrt{1+\alpha^2R^2})$ . It follows that  $k_n = -\sin(2\psi)/\alpha\ell^2$ ,  $k_g = \partial_s \psi + (R\sin \psi)/\ell^2$ , and  $\tau_g = (1-2\cos^2 \psi)/\alpha\ell^2$ , with  $k^2 = k_n^2 + k_g^2$  and  $\ell^2 = \alpha^{-2} + R^2$ . Once the shape is determined, the force is F = dE/dZ.

We first make analytical predictions about F(z). Assuming  $z \ll a$ ,  $B \ll \gamma a^2$ , and  $p \to \infty$ , we find  $F = k_s z$ , where the effective spring constant is

$$k_{\rm s} = \pi \gamma / (2a) + \pi^2 / 4\sqrt{\gamma B / a^4} +, \cdots$$
 (2)

This expression qualitatively reproduces the experimental finding that smaller membranes are effectively stiffer. Using independently determined values for a, B and  $\gamma$  we find the above approximation is in quantitative agreement with the experiments for membranes with diameter  $\gtrsim 10~\mu m$  [Fig. 3(b)]; a nonzero value of the edge bending stiffness B is essential for obtaining this agreement. As membrane size becomes comparable to twist penetration length, the plateau regime disappears and the theory underestimates the effective membrane stiffness.

The model also provides an estimate of the magnitude of the plateau regime. When  $z\gg a$ , we approximate the membrane as a twisted rectangular strip in the achiral case  $c^*=0$  and find  $F\to 2\gamma-\bar\kappa^2/B$ ; the force saturates at a value independent of the membrane size. Line tension, Gaussian curvature modulus, and edge bending stiffness are primarily responsible for the force in the first linear and plateau regimes. Including the chiral coupling  $c^*$  term yields a more complicated form for the asymptotic force but a similar numerical value for experimentally relevant parameters.

All parameters of our model are determined independently, allowing us to numerically calculate the forceextension curves as a function of membrane diameter (Fig. 3). For the three largest membranes, the discrepancy between theory and experiment is comparable to the 20% variation between different experiments. For the two smallest membranes, which do not exhibit the plateau regime, the agreement is poor. In this regime, the small extension Hooke's law regime seems to directly transition to the second linear regime, which is not treated by our theory. Furthermore, since our effective model has no fitting parameters, one should not expect uniformly good quantitative agreement across a range of membrane sizes. Most of these parameters are only well defined when the half-micron twist penetration depth is significantly smaller than the membrane size. Numerical results showed quantitative agreement with experimentally measured force and pitch for two differently sized fd-wt membranes with lower edge tension (Fig. 4). Here, the agreement between theory and experiment for the force-extension curve is better due to the presence of plateaus. The agreement for the pitch-extension curve is also reasonable once the extension is large enough for an accurate measure of the twist. We note that the model predicts the ribbon twists continuously as a function of extension and a nonzero value of  $c^*$  was required for visible twisting, implying that microscopic chirality is essential for producing ribbons in the range of applied extensions.

To summarize, in the absence of external force diskshaped colloidal membranes are stabilized by line tension and edge bending energy, despite the tendency of chirality and positive Gaussian modulus  $\bar{k}$  to induce twisted shapes. Pulling on the membrane increases its perimeter, and forming helical edges lowers the twist energy enough to overcome the additional cost in edge length and edge bending. The predictions of the proposed effective theory are in semiquantitative agreement with the experimental measurements. Quantitative discrepancies occur in the regime where the theory is expected to break down. Future theoretical work should account more explicitly for the liquid crystalline degrees of freedom of the constituent rods and remove the constraint of fixed area; generalizing the theory in this way may allow us to address the second linear regime. Experimentally, it has been demonstrated that lowering the edge tension by increasing the chirality of the constituent rods spontaneously transforms disk-like membranes into twisted ribbons [18]. The methods developed here could be used to map the free energy landscape associated with such morphological transitions.

This work was supported in part by the National Science Foundation through Grants No. MRSEC-1420382 (A. B., Z. D., L. L. J., R. A. P., and T. R. P.), No. BMAT-1905384 (A. B., M. J. Z., and Z. D.), and No. CMMI-1634552 (L. L. J., R. A. P., and T. R. P.). We are grateful to Megan Kerr for helpful discussions.

- \*Present address: Flatiron Institute, Center for Computational Biology, 162 5th Avenue, New York, New York 10010, USA.
- [1] C. Darwin, *The Movements and Habits of Climbing Plants* (J. Murray, London, 1875).
- [2] H. C. Berg, The rotary motor of bacterial flagella, Annu. Rev. Biochem. **72**, 19 (2003).
- [3] P. Burkhard, J. Stetefeld, and S. V. Strelkov, Coiled coils: A highly versatile protein folding motif, Trends Cell Biol. 11, 82 (2001).
- [4] B. Brodsky and J. A. M. Ramshaw, The collagen triple-helix structure, Matrix Biol. **15**, 545 (1997).
- [5] J. M. Schnur, Lipid tubules: A paradigm for molecularly engineered structures, Science **262**, 1669 (1993).
- [6] R. Oda, I. Huc, M. Schmutz, S. J. Candau, and F. C. MacKintosh, Tuning bilayer twist using chiral counterions, Nature (London) 399, 566 (1999).

- [7] A. R. Studart and R. M. Erb, Bioinspired materials that self-shape through programmed microstructures, Soft Matter 10, 1284 (2014).
- [8] S. Armon, E. Efrati, R. Kupferman, and E. Sharon, Geometry and mechanics in the opening of chiral seed pods, Science **333**, 1726 (2011).
- [9] Y. Klein, E. Efrati, and E. Sharon, Shaping of elastic sheets by prescription of non-Euclidean metrics, Science 315, 1116 (2007).
- [10] M. D. Lima, S. Fang, X. Lepró, C. Lewis, R. Ovalle-Robles, J. Carretero-González, E. Castillo-Martínez, M. E. Kozlov, J. Oh, N. Rawat *et al.*, Biscrolling nanotube sheets and functional guests into yarns, Science 331, 51 (2011).
- [11] E. D. Sone, E. R. Zubarev, and S. I. Stupp, Semiconductor nanohelices templated by supramolecular ribbons, Angew. Chem., Int. Ed. Engl. **41**, 1705 (2002).
- [12] S. Srivastava, A. Santos, K. Critchley, K.-S. Kim, P. Podsiadlo, K. Sun, J. Lee, C. Xu, G. D. Lilly, S. C. Glotzer et al., Light-controlled self-assembly of semiconductor nanoparticles into twisted ribbons, Science 327, 1355 (2010).
- [13] P. Cluzel, A. Lebrun, C. Heller, R. Lavery, J.-L. Viovy, D. Chatenay, and F. Caron, DNA: An extensible molecule, Science 271, 792 (1996).
- [14] S. B. Smith, Y. Cui, and C. Bustamante, Overstretching B-DNA: The elastic response of individual double-stranded and single-stranded dna molecules, Science **271**, 795 (1996).
- [15] B. Smith, Y. V. Zastavker, and G. B. Benedek, Tension-Induced Straightening Transition of Self-Assembled Helical Ribbons, Phys. Rev. Lett. 87, 278101 (2001).
- [16] E. Barry and Z. Dogic, Entropy driven self-assembly of nonamphiphilic colloidal membranes, Proc. Natl. Acad. Sci. U.S.A. 107, 10348 (2010).
- [17] Y. Yang, E. Barry, Z. Dogic, and M. F. Hagan, Self-assembly of 2d membranes from mixtures of hard rods and depleting polymers, Soft Matter 8, 707 (2012).
- [18] T. Gibaud, E. Barry, M. J. Zakhary, M. Henglin, A. Ward, Y. Yang, C. Berciu, R. Oldenbourg, M. F. Hagan, D. Nicastro et al., Reconfigurable self-assembly through chiral control of interfacial tension, Nature (London) 481, 348 (2012).
- [19] M. J. Zakhary, T. Gibaud, C. N. Kaplan, E. Barry, R. Oldenbourg, R. B. Meyer, and Z. Dogic, Imprintable membranes from incomplete chiral coalescence, Nat. Commun. 5, 3063 (2014).
- [20] P. Sharma, A. Ward, T. Gibaud, M. F. Hagan, and Z. Dogic, Hierarchical organization of chiral rafts in colloidal membranes, Nature (London) **513**, 77 (2014).
- [21] T. Gibaud, C. Nadir Kaplan, P. Sharma, M. J. Zakhary, A. Ward, R. Oldenbourg, R. B. Meyer, R. D. Kamien, T. R. Powers, and Z. Dogic, Achiral symmetry breaking and positive gaussian modulus lead to scalloped colloidal membranes, Proc. Natl. Acad. Sci. U.S.A. 114, E3376 (2017).
- [22] C. N. Kaplan, H. Tu, R. A. Pelcovits, and R. B. Meyer, Theory of depletion-induced phase transition from chiral smectic-a twisted ribbons to semi-infinite flat membranes, Phys. Rev. E 82, 021701 (2010).

- [23] H. Tu and R. A. Pelcovits, Theory of self-assembled smectic-A crenellated disks: Membranes with cusped edges, Phys. Rev. E 87, 032504 (2013).
- [24] L. L. Jia, M. J. Zakhary, Z. Dogic, R. A. Pelcovits, and T. R. Powers, Chiral edge fluctuations of colloidal membranes, Phys. Rev. E 95, 060701(R) (2017).
- [25] E. Barry, Z. Dogic, R. B. Meyer, R. A. Pelcovits, and R. Oldenbourg, Direct measurement of the twist penetration length in a single smectic-A layer of colloidal virus particles, J. Phys. Chem. B 113, 3910 (2008).
- [26] P.B. Canham, The minimum energy of bending as a possible explanation of the biconcave shape of the human red blood cell, J. Theor. Biol. **26**, 61 (1970).
- [27] W. Helfrich, Elastic properties of lipid bilayers: Theory and possible experiments, Z. Naturforsch. 28C, 693 (1973).
- [28] Z. Dogic and S. Fraden, Development of model colloidal liquid crystals and the kinetics of the isotropic–smectic transition, Phil. Trans. R. Soc. A 359, 997 (2001).
- [29] E. Grelet and S. Fraden, What is the Origin of Chirality in the Cholesteric Phase of Virus Suspensions?, Phys. Rev. Lett. 90, 198302 (2003).
- [30] F. Tombolato, A. Ferrarini, and E. Grelet, Chiral Nematic Phase of Suspensions of Rodlike Viruses: Left-Handed Phase Helicity from a Right-Handed Molecular Helix, Phys. Rev. Lett. 96, 258302 (2006).
- [31] See Supplemental Material at http://link.aps.org/ supplemental/10.1103/PhysRevLett.125.018002 for detailed experimental methods, which includes Refs. [32–37].
- [32] M. J. Zakhary, P. Sharma, A. Ward, S. Yardimici, and Z. Dogic, Geometrical edgeactants control interfacial bending rigidity of colloidal membranes, Soft Matter 9, 8306 (2013).
- [33] E. J. Wood, in *Molecular Cloning. A Laboratory Manual*, edited by T. Maniatis, E. F. Fritsch, and J. Sambrook (Cold Spring Harbor Laboratory, New York, 1982).
- [34] E. Barry, D. Beller, and Z. Dogic, A model liquid crystalline system based on rodlike viruses with variable chirality and persistence length, Soft Matter 5, 2563 (2009).

- [35] A. W. C. Lau, A. Prasad, and Z. Dogic, Condensation of isolated semi-flexible filaments driven by depletion interactions, Europhys. Lett. 87, 48006 (2009).
- [36] E. Barry, Z. Hensel, Z. Dogic, M. Shribak, and R. Oldenbourg, Entropy-Driven Formation of a Chiral Liquid-Crystalline Phase of Helical Filaments, Phys. Rev. Lett. **96**, 018305 (2006).
- [37] M. W. Allersma, F. Gittes, M. J. deCastro, R. J. Stewart, and C. F. Schmidt, Two-dimensional tracking of ncd motility by back focal plane interferometry, Biophys. J. 74, 1074 (1998).
- [38] M. Siavashpouri, C. H. Wachauf, M. J. Zakhary, F. Praetorius, H. Dietz, and Z. Dogic, Molecular engineering of chiral colloidal liquid crystals using DNA origami, Nat. Mater. **16**, 849 (2017).
- [39] E. Memet, F. Hilitski, M. A. Morris, W. J. Schwenger, Z. Dogic, and L. Mahadevan, Microtubules soften due to cross-sectional flattening, eLife 7, e34695 (2018).
- [40] H.-T. Jung, S. Y. Lee, E. W. Kaler, B. Coldren, and J. A. Zasadzinski, Gaussian curvature and the equilibrium among bilayer cylinders, spheres, and discs, Proc. Natl. Acad. Sci. U.S.A. 99, 15318 (2002).
- [41] M. Hu, J. J. Briguglio, and M. Deserno, Determining the Gaussian curvature modulus of lipid membranes in simulations, Biophys. J. **102**, 1403 (2012).
- [42] A. J. Balchunas, R. A. Cabanas, M. J. Zakhary, T. Gibaud, S. Fraden, P. Sharma, M. F. Hagan, and Z. Dogic, Equation of state of colloidal membranes, Soft Matter 15, 6791 (2019)
- [43] M. Kléman, Points, Lines, and Walls (John Wiley & Sons, Chichester, 1983).
- [44] R. D. Kamien, The geometry of soft materials: A primer, Rev. Mod. Phys. **74**, 953 (2002).
- [45] The MATLAB routine fmincon was used to perform the optimization.
- [46] U. Seifert, K. Berndl, and R. Lipowsky, Shape transformations of vesicles: Phase diagram for spontaneous-curvature and bilayer-coupling models, Phys. Rev. A 44, 1182 (1991).